HHS Public Access

Author manuscript

Biofabrication. Author manuscript; available in PMC 2021 March 30.

Published in final edited form as:

Biofabrication. ; 11(1): 015003. doi:10.1088/1758-5090/aae543.

Optimization of collagen type I-hyaluronan hybrid bioink for 3D bioprinted liver microenvironments

Andrea Mazzocchi[1,2], **Mahesh Devarasetty**[1], **Richard Huntwork**[1], **Shay Soker**[1,2,3,4], **Aleksander Skardal**[1,2,3,4]

[1]Wake Forest Institute for Regenerative Medicine, Wake Forest School of Medicine, 391 Technology Way, Winston-Salem, NC, 27101, United States of America

[2]Virginia Tech-Wake Forest School of Biomedical Engineering and Sciences, Wake Forest School of Medicine, Medical Center Boulevard, Winston-Salem, NC, 27157, United States of America

[3]Department of Cancer Biology, Wake Forest School of Medicine, Medical Center Boulevard, Winston-Salem, NC, 27157, United States of America

[4]Comprehensive Cancer Center at Wake Forest Baptist Medical, Medical Center Boulevard, Winston-Salem, NC, 27157, United States of America

Abstract

Current 3D printing of tissue is restricted by the use of biomaterials that do not recapitulate the native properties of the extracellular matrix (ECM). These restrictions have thus far prevented optimization of composition and structure of the *in vivo* tissue microenvironment. The artificial nature of currently used biomaterials affects cellular phenotype and function of the bioprinted tissues, and results in inaccurate modeling of disease and drug metabolism significantly. Collagen type I is the major structural component in the ECM, and is widely used as a 3D hydrogel, but is less applicable for 3D bioprinting due to low viscosity and slow polymerization. We have hypothesized that a combination of hyaluronic acid with collagen I yields a bioink with the properties required for extrusion bioprinting, while supporting native cell–matrix interactions and preservation of the native microenvironment properties. To test this hypothesis, we tested the viscoelastic properties of three bioink formulations –2:1, 3:1, and 4:1 collagen type I to hyaluronic acid, and examined cellular behavior in order to determine an optimal formulation that allows for bioprinting while supporting biological activity. We then employed this formulation to bioprint 3D liver tissue constructs containing primary human hepatocytes and liver stellate cells and tested the effects of acetaminophen, a common liver toxicant. Our results have shown that the combination of methacrylated collagen type I and thiolated hyaluronic acid yield a simple, printable bioink that allows for modulation that was directly related to stromal cell elongation. Further, the bioink adequately allowed for implementation as a support hydrogel for hepatocytes which were able to remain viable over two weeks and responded to drug treatment appropriately.

askardal@wakehealth.edu.

Competing Interests

The authors have not competing interests to disclose.

Supplementary material for this article is available online

Keywords

bioink; 3D bioprinting; liver; microenvironment; extracellular matrix; collagen; hyaluronic acid

Introduction

In the last two decades, it has become apparent that three-dimensional (3D) culture can have a variety of benefits over traditional two-dimensional (2D) cell culture [1–3]. Use of 3D culture allows for customized topography, stiffness, and material composition, which can facilitate cell–cell and cell–matrix interactions vital for tissue formation and function [3, 4]. Importantly, it allows cells to interact in all directions with extracellular matrix (ECM) components and neighboring cells allowing tissue-like structures to form rather than being restricted by substrate and media interfaces found in traditional 2D cell culture [4]. Although 3D culture is not new, the use of biomaterials in 3D culture settings has been limited by the inability to make complex biological structures and designs due to size, material, compositional, and technological constraints [5]. In parallel, advancements in bioprinting have decreased costs and increased the accessibility of commercial benchtop bioprinters allowing straightforward extrusion of materials and efficient development of simple printed tissue constructs. Continued advancements have allowed the creation of more complex 3D structures using multiple biomaterials and cell types in combination [6]. The numerous available bioprinting modalities, including inkjet, laser-assisted, and extrusion bioprinting, have their own specific benefits which facilitate customization of prints for numerous applications [7]. Extrusion bioprinting, which is currently the most utilize bioprinting modality in biomedical research, specifically allows for bioink and tissue customization by placing few restrictions on cells used [6]. However, current biomaterials are restrictive in that they are either easy to print or ideal for cell culture, but typically not both [8]. Hydrogel bioinks for extrusion bioprinting must be viscous enough to print, but elastic enough to maintain their structure, while also maintaining cell viability and supporting cellular function [8, 9].

Hydrogels are broadly defined as polymer networks that are often crosslinked together and have the ability to swell in aqueous environments [10]. There are many biomedical applications of hydrogels which both include and in turn contributed greatly to stem cell-based therapy, tissue engineering and regenerative medicine, organoid formation, pathophysiological studies, and drug screening [10, 11]. Of these applications, many leverage the 3D nature of hydrogels to create tissues or scaffolds and may be well suited for bioprinting through utilization of bioinks. Bioinks are more specifically defined as materials used in 3D bioprinting that allow for spatially controlled patterning of cells and biocompatible materials; these materials include hydrogels [9]. Some commercial bioinks have the previously described ideal properties, but they fail to offer physiologically relevant ECM components for replication of cell–cell and cell–matrix interactions found *in vivo.* The most common bioinks are typically comprised of polyethylene glycol (PEG), collagen, alginate, hyaluronic acid, gelatin, fibrin, or poly-caprolactone [9, 12]. Each bioink has unique properties that can either benefit or hinder bio-printability or tissue development [8, 12]. With the exception of collagen, each biomaterial described above requires the addition

of a crosslinker and crosslinking speed can vary significantly [9, 12]. Crosslinking components and time required for crosslinking can both adversely affect cells and should be appropriately balanced with the benefits of the biocompatibility of the bioink being used [13, 14]. Additionally, some materials do not provide physiologically relevant cell adhesion points and force cell–cell interactions (e.g. alginate and PEG) [15]. Although this is an improvement over standard 2D culture, it is still limiting and may not represent the cellular microenvironment of the target *in vivo* tissue. Materials that allow for more ideal cell–matrix interactions are often challenging to print, the best example being collagen [14]. Although collagen is an ideal material for *in vivo*-like tissue replication, it is a poor bioink because it has time- and temperature-sensitive crosslinking [12]. Starting as a low viscosity liquid, neutralized collagen begins to exhibit fiber self-assembly unless solution temperature is well controlled. Within 30 min hydrogen bond formation between collagen fibers produces a solidified gel. This is problematic for bioprinting because collagen crosslinking is continuous prior to reaching gel state, meaning that it is difficult to control, resulting in variable viscosity and elastic modulus throughout the printing process or solution heterogeneity. Nevertheless, because collagen is the most abundant component in the ECM of nearly every tissue in the human body, there is great impetus to develop bioink biomaterials comprised of collagen with which 3D tissue constructs can be bioprinted.

A physiologically representative 3D microenvironment is vital to the development of *in vitro* tissue models, such as liver [16, 17]. Liver tissue is complex: the organization of hepatocytes, hepatic stellate cells, and ECM are all required to appropriately create the microenvironment of hepatic lobules [18]. This has been exemplified in the inability of 2D hepatocyte cultures to support even minor liver functions [19, 20]. Hepatocytes are often unable to maintain function and survive in 2D for extended periods potentially due to the inability to form *in vivo*-like structures; this limits the utility of 2D systems in drug screening and disease modeling studies [20, 21]. However, placing cultures into 3D form factors has not completely eliminated the challenges of culturing hepatocytes. Current models are primarily comprised of cell aggregates with little to no additional ECM components. Of those using ECM components, one of primary interest is collagen type I (COL I) as it has ideal properties for cell reorganization and has been shown to allow for useful structures to form with regard to liver function and organ modeling [22–24]. As previously discussed, COL I alone is not advantageous for printing and thus a multi-component hybrid bioink is a potential solution for achieving ideal physiological relevance and bio-printability.

In this study, we combined methacrylated COL I with thiolated hyaluronic acid (HA) to produce a bioink that is printable with physiologically relevant native ECM-derived components. We hypothesized that an intermediate ratio of COL I to HA is both best for printing and tissue organization in comparison to an industry standard HA/gelatin hydrogel. To test this hypothesis, matrix organization, printing properties, and cell biocompatibility of the bioinks were analyzed and compared. Two hepatic stellate cell types were used within three bioink formulation made of COL I and HA for cell viability and functional testing. Further, a heterocellular liver model was bioprinted to assess whether the bioink could support liver function and drug response. To the best of our knowledge, this is the first COL I/HA hybrid bioink for 3D bioprinting. Through utilization of a functioning liver model, we

have been able to show strong support for the use of COL I/HA hybrid bioinks in bioprinting applications.

Materials and methods

Bioink formulation

Bioink formulations were prepared by combining methacrylated COL I and thiolated HA in three ratios for initial testing and characterization (as illustrated in figure 1(A)). Methacrylated COL I (collagen) was prepared at 6 mg ml^{-1} per manufacturer's instructions excluding the provided photoinitiator (Advanced Biomatrix, San Diego, CA). Prior to use with HA, collagen was neutralized using manufacturer provided neutralization solution at 85 μl of solution per milliliter of collagen. HA was prepared at 2 mg ml^{-1} by re-suspending Heprasil (heparinized and thiolated HA, ESI BIO, Alameda, CA) in 1 ml deionized water with 0.1% w/v photoinitiator (Sigma Aldrich, 410896, St. Louis, MO). Three ratios of collagen to HA were used for optimization studies (2:1, 3:1, and 4:1).

Rheology characterization

A Discovery HR-2 Rheometer (TA Instruments, New Castle, DE) with an 8 mm parallel plate geometry was used to collect the rheological data. After hydrogel precursor preparation, 200 μl of the reaction mixture was transferred into a 12 mm diameter × 5 mm depth PDMS well. The PDMS well containing the reaction mixture was then either measured as is or exposed to ultraviolet (UV) radiation of 1.9 W cm^{-2} for 2 s at a distance of 1 cm, resulting in instantaneous photo-initiated polymerization and hydrogel formation. To ensure standard conditions across all experiments the geometry was lowered into the gels until a calibration normal force of 0.04 N was achieved. Following, an oscillatory shear-stress sweep test (0.6–10.0 Pa, 1.0 Hz, 25 °C) was applied to hydrogels of each collagen to HA ratio (2:1, 3:1, 4:1). This experiment was repeated in triplicate for each condition. Average values for storage and shear loss moduli, $\boldsymbol{G'}$ and $\boldsymbol{G''}$, respectively, were determined for each condition.

Bioprinting

An Allevi 2 bioprinter (Allevi, Philadelphia, PA) with 28G blunt end needle was used for printability testing and liver model printing. Previous to any printing, bioink solutions were combined and allowed to rest on ice for 45 min. A single bioink layer was extruded at 4 kPa pressure with a speed of 50 mm s^{-1} in a four spoke shape created via 3D software. Printability testing was performed using bioinks without cells and printed onto 5 cm tissue culture plastic dishes and then imaged, after which measurements for quantification were taken using ImageJ software. Liver model printing was performed in 6-well tissue culture plastic plates with a thin polydimethylsiloxane (PDMS) coating to prevent cell outgrowth onto plastic substrates. All printed structures were crosslinked using UV irradiation immediately after printing for 10 s with UV light being passed over the entire structure during that time.

L × 2 and aHSC stellate cell culture

A human hepatic stellate cell line (L × 2) and primary fetal activated hepatic stellate cells (aHSC) were independently cultured on tissue culture plastic plates and used between passages 7 and 10 for experimentation [25–27]. Both cell types were expanded until reaching 70%–80% confluency in Dulbecco's Modified Eagle Medium with 10% fetal bovine serum and 200 μml^{-1} penicillin and streptomycin (DMEM-10) (Gibco, Gaithersburg, MD). Cells were then retrieved from culture for bioink experiments using 0.05% Trypsin-EDTA (ThermoFisher Scientic, Waltham, MA) [27]. For bioink cultures, constructs were made using L × 2 or aHSCs at 5 million cells ml^{-1}. Cells were combined with bioink and 10 μl droplets of cell-gel solution were individually deposited into 48-well plastic plates that had been previously coated in a thin layer of PDMS. Constructs were sustained for 7 d with media changes on days 3 and 6 with DMEM-10. On day 7 experimentation was concluded and constructs were sacrificed for LIVE/DEAD cell viability assay (ThermoFisher Scientic, Waltham, MA) and fixation for histological processing. In addition to collagen/HA bioink formulations, an HA/gelatin hydrogel (Hystem-HP, ESI BIO) was also used for cell culture as a baseline for viability comparisons, and was prepared according to the manufacturer's instructions.

Hepatocyte cell culture and liver model

Primary human hepatocytes (Triangle Research Labs, Morrisville, NC) were bioprinted for the study of functionality within the bioink. Hepatocytes were thawed from a frozen cryovial and re-suspended in 10 ml hepatocyte complete media (HCM) (Lonza, Walkersville, MD). Hepatocytes were counted, centrifuged, and re-suspended in 3:1 (collagen:HA) bioink at 5 million cells ml^{-1}. Four-spoke structures were printed using the same design as that of the printability testing and contained hepatocytes that were grown for 15 d. Printing was done at 4 kPa pressure with a speed of 50 mm s^{-1} in a single layer. On day 6, 100 mM acetaminophen (APAP) was added to two printed liver structures. Triplicate controls were maintained in parallel, and fresh media with or without APAP based on experimental group was refreshed every three days throughout the remainder of the experiment.

Viability assays

LIVE/DEAD cell viability assays were performed using calcein AM and ethidium homodimer-1 reagents (1:500 each) in DPBS (ThermoFisher Scientific). Samples were incubated with the staining solution at 37 °C for 30 min after which they were washed and stored in DPBS before imaging on a Leica TCS LSI macro-confocal microscope (Leica, Wetzlar, Germany). Live and dead stained cells were counted manually and a ratio of live to dead cells was calculated for each cell condition. Cellular aspect ratios were calculated from thresholded LIVE/DEAD images using the Analyze Particles measurement in Fiji [28].

Histological processing

Stellate cell tissue constructs and bioprinted liver structures were washed twice with DPBS and fixed with 4% paraformaldehyde for 1 h then additionally washed twice with DPBS. Cultures were histologically processed, paraffin embedded, and sectioned at 5 μm thickness. Hemotoxylin and eosin (H&E) and picrosirus red staining was conducted on each of the

stellate cell constructs conditions (ab150681, Abcam, San Francisco, CA), while H&E was conducted on bioprinted liver models. Images were captured on an Olympus BX63 brightfield microscope with picrosirus red images captured using polarized light.

Functionality assays

Media aliquots were collected from liver models of $n = 2$ or greater every 3 d for a total of 15 d in culture. Collected aliquots were stored at −80 °C until assays were performed. Human albumin (Abcam) and glutathione s-transferase alpha (alpha-GST, Oxford Biomedical Research, Rochester Hills, MI) ELISAs and a human urea (Abcam) colorimetric assay were performed following the manufacturers' instructions.

Statistical analysis

Rheology testing was done with $n = 6$ samples per conditions. A student's t-test was employed to compare storage modulus and loss modulus between each of the materials previous to crosslinking (extrusion moduli) and after crosslinking as well as between each other. Bioprintability studies were done using $n = 8$ samples per material condition. ANOVA was employed to compare between each of the formulations. LIVE/DEAD viability assay groups were compared using student's t-test, $n = 9$ images ($n = 3$ constructs, 3 images per construct). Hepatocyte structures were $n = 3$ for untreated conditions and $n = 2$ for APAP treated conditions. Student's t-test was used for comparison of each condition at each time point.

Results

Physical characterization

Characterization of the bioink compositions; COL I: HA 2:1, 3:1, and 4:1, was performed via shear storage and loss moduli measurements before and after UV exposure to induce crosslinking (figure 1). The shear storage modulus ($\mathbf{G}'$) represents the elastic component of a material and specifically measures the stored energy of the material. The shear loss modulus ($\mathbf{G}''$) represents the viscous component of the material and measures the energy released from the material. These properties are important for biomaterials used for 3D printing because they determine the interplay between the ability of a material to flow versus to maintain its shape. Previously, it has been determined that materials with greater $\mathbf{G}'$ than $\mathbf{G}''$ are more printable than those with large $\mathbf{G}''$ components as long as the material remains able to flow. To determine if a material is applicable for bioprinting, the loss tangent is used which is calculated as $\mathbf{G}''/\mathbf{G}'$ [29]. Materials are more elastic as the loss tangent decreases and more viscous as it increases [29, 30]. Previously characterized commercial bioinks have loss tangents between 0.30 and 0.45 during printing and decrease to below 0.2 when crosslinked [31]. Since the biomaterial is first extruded and then crosslinked by UV light, we performed moduli measurements on each formulation before exposure to UV, in order to determine the physical characteristics as they would be printed, and after UV crosslinking. However, it should be noted that given the nature of the thiolated HA and methacrylated collagen, some pH-driven crosslinking may occur spontaneously. Bioinks were left on ice for 45 min prior to testing in order to allow for any linking driven by thiol-methacrylate reactions (figure 1(A)). All three formulations show a greater storage modulus in

comparison to loss modulus but appropriately balance each other by yielding loss tangents between 0.29 and 0.33 (figure 1(B)). After UV mediated crosslinking of the materials, the shear storage modulus ($\mathbf{G}'$) is increased significantly across all conditions when compared to uncrosslinked materials ($p < 0.005$). The shear loss modulus however does not significantly change before and after UV crosslinking, and due to these changes, all loss tangents decreased below 0.1, indicating the material has become more elastic (figures 1(B), (C)). In the crosslinked form, each of the bioinks (2:1, 3:1, 4:1 COL I: HA) maintain their shape, are able to be grasped with forceps, and maintain integrity for an observed time of greater than 60 d in DPBS.

Printability measures

We assessed printability of each formulation by measuring stability of bioinks after mixing of COL I and HA and by printing a set structure using a benchtop extrusion bioprinter (figure 2(A)). A 4-spoke structure (illustrated in figure 2(A)) was used to test the ability of the bioinks to form measurable structures in both straight and curved lines. Printing of each set of structures was conducted over a period of 45 min with 8 structures being produced for each bioink formulation (2:1, 3:1, 4:1 COL I:HA). Time included removal and replacement of plates. Each of the structures was immediately crosslinked after printing. For both the 2:1 and 3:1 mixtures, the printed material was visually homogenous throughout the 30 min printing duration. Printability of bioinks extended to approximately 45 min within the bioprinter. The 4:1 mixture displayed visual phase separation after 30 min. Overall consistency of each of the printed structures following UV exposure was assessed by measuring the diameter in two locations, the arm length and width of all 4 arms (4 measurements per structure) (figure 2(E)). Within the 30 min printing period, each of the bioink mixtures appear to produce similar structures and there were no statistically significant differences found.

Cell viability and collagen characterization

Bioprinting is intended for creating supportive microenvironments that should facilitate cell viability and function. LIVE/DEAD assays were conducted to determine biocompatibility of each bioink mixture, and that of a commercially available hydrogel comprised of HA and gelatin [32, 33]. L × 2 and aHSCs are hepatic stellate cells and were chosen in order to test their ability to interact with their microenvironment and the ECM [34]. Both of the cell types were grown in each of the four formulations (HA/gelatin, 2:1, 3:1, 4:1 COL I:HA) for 7 d and a LIVE/DEAD cell viability assay was performed. The stained structures were imaged using macro-confocal microscopy and the percentage of viable cells in each condition was calculated using manual cell counts from each image collected for each of the conditions (figures 3(A), (D)). We observed >80% of viable cells for each of the formulations, indicating that all were able to support cell viability (figures 3(B), (E)). The microscope images additionally show cell/matrix interactions of the activated stellate cells versus the more naïve L × 2 cells (figures 3(A), (D)) [34, 35]. Interestingly, the 3:1 and 4:1 formulations induced more pronounced cell shape changes in aHSCs, suggesting that an increase in COL I supports better cell–matrix attachments and cell spreading. Quantification of cell aspect ratio (figures 3(C), (F)) support this observation as aHSCs in the 3:1 and 4:1 formulation display higher aspect ratios, or more elongation, when compared to HA/gelatin

culture conditions. No differences in aspect ratio were measured in L × 2 cells. To further assess cell–matrix interaction we performed H&E and Picrosirus Red (PSR) staining of the printed constructs. L × 2 cells behave similarly in all bioink formulations as well as the commercial HA/gelatin hydrogel with all cells forming aggregates which do not appear to be remodeling or interacting with the surrounding collagen (figures 4(A), (C)). Conversely, aHSCs exhibit elongation within the collagen based bioinks (3:1 and 4:1) which further indicates an increase in cell–matrix interaction with cultures including these cells (figure 4(C)). Additionally, PSR staining was used to characterize collagen remodeling (fiber bundling) in these structures (figures 4(B), (D)). Red and orange signal denotes bundled collagen, which can be observed around cells in all bioink formulations but is absent in the HA/gelatin samples.

Liver model

Hepatocytes are integral for liver function and make up approximately 80% of the entire liver to carry out metabolic and detoxifying activities. Hepatocytes, although well characterized, can be challenging to grow *in vitro* and have low viability and minimal function if not cultured in the correct environment. Current *in vitro* techniques for use of hepatocytes in drug toxicity testing and metabolomics are primarily seeding hepatocytes on COL I gels, which maintain cell viability for a limited time [22, 36–37]. Bioprinting hepatocytes in 3D structures offers a novel platform for *in vitro* culture and testing of hepatocyte function and response. To determine viability and functionality of hepatocytes within the bioink, they were bioprinted in the 3:1 COL I to HA formulation. The 3:1 bioink formulation was utilized as it contained a high concentration of collagen while maintaining consistent printability. Bioprinted constructs were maintained in culture for 6 d and subsequently, hepatocyte functionality was determined by exposing the constructs to an hepatic toxicant, acetaminophen (APAP, 100 μM) and measuring the levels of albumin, urea, α-GST, and lactic acid dehydrogenase (LDH) in the media over time. Significant decreases in both urea and albumin levels were observed at day 9 and continued to decrease through day 15 for the APAP treated conditions, compared with stable levels in the untreated constructs (figures 5(A), (B)). Interestingly, the levels of α-GST, a detoxification protein, increased at day 9, 3 d post APAP addition, but subsequently decreases by day 12, likely due to cell death (figure 5(C)). The high levels of α-GST after 3 d in culture, and prior to drug addition, may be due to cell-stress experienced during the printing procedure that led to upregulation of α-GST expression. In addition, levels of LDH, a marker of liver damage, also peak due to printing-related stress, but fall to nominal levels by day 6. APAP treated constructs demonstrate decreasing LDH activity, again likely due to toxicity related cell death. Untreated conditions maintain steady LDH until day 15 when levels begin to increase. Increases in LDH and α-GST at day 15 indicates this period may be nearing the culture limit, however LIVE/DEAD assay was conducted and cultures remained viable (supplementary figure 1 is available online at stacks.iop.org/BF/11/015003/mmedia). Taken together, these results demonstrate appropriate response to a well-known and characterized liver toxin, indicating the bioink is sufficient to both maintain hepatocyte viability and support physiologic response to drugs. Histological staining (H&E) demonstrated greater cellularity in untreated constructs, while drug-treated conditions show loss of cellularity (figure 5(D)).

Discussion

Bioprinting has made substantial advances in the past two decades, however biomaterials ideal for both printing and development of cellular microenvironments have been limited [8]. However, by combining previously characterized biomaterials into hybrid bioinks, printability can be optimized using physiologically relevant materials that cells will recognize as actual ECM rather than inert or synthetic alternatives. A current limitation to most commercial bioinks is that they are lacking in true ECM-like components. This can prevent cells from recognizing and interacting with their microenvironment as well as restrict the development of *in vivo*-like tissues and morphologies. In this study, methacrylated COL I has been combined with thiolated hyaluronic acid to produce a novel bioink that is both easy to use for bioprinting and supports cellular viability and function. These properties were then deployed to biofabricate a simple *in vitro* human liver model yielding satisfactory functionality.

Printability was determined through rheological and printed structure measurements. By measuring loss and storage moduli previous to and after UV radiation crosslinking and further calculating the loss tangent, it was shown that each of the materials (2:1, 3:1, 4:1 COL I:HA) exhibited the same mechanical properties. All formulations had greater fluid than elastic features previous to crosslinking. This indicates that each of the materials was able to flow in the viscous/liquid phase. Yet, because the storage modulus component was high enough, the bioink could hold its shape for a period of time following printing, prior to UV crosslinking. After crosslinking, the loss modulus was decreased for each of the materials and the storage modulus was significantly increased. This change indicates the transition from a liquid that is able to flow to a material that is able to maintain its shape permanently and was observed for each of the materials. Printability testing was additionally conducted on each of the three materials to determine which would be ideal for printing. While each of the three was able to print structures of the appropriate shape with minimal variation for 30 min or more, it was found that at room temperature the 4:1 bioink began phase separating and was no longer homogenous, with collagen bundles forming in solution. Separation of the bioink was a major consideration when determining the ideal bioink for liver microenvironment printing. From determining the moduli and conducting printability testing on each of the bioinks, it was determined that each of the bioinks behaved the same and no significant differences were measured. However, longevity of printing is limited with the 4:1 formulation, which reduces its utility as a bioink. Due to the greater amount of COL I within the formulation, collagen is likely limited in its interaction with HA and instead primarily interacts with itself, at room temperature this quickly leads to bundling of the collagen within the bioink.

Cell viability and characterization of collagen within the bioinks was further studied to determine which would be most ideal for cells. Using LIVE/DEAD cell viability assays, it was shown that each of the bioinks was able to adequately support cells compared to other commercial, previously characterized hydrogels. It was found that each of the bioinks (2:1, 3:1, 4:1 COL I:HA) maintained high cellular viability and were comparable to other 3D biomaterials. Although no differences in viability were measured, LIVE/DEAD cell viability assay images indicated differences in cell morphology. HA/gelatin samples elicited no

elongation from aHSCs or L × 2 cells—both of which are characterized by their ability to interact with their microenvironment—and cells tended to favor cell–cell interactions in this hydrogel [38]. An increase in collagen content increased elongation of aHSCs. Collagen presence and bundling was shown through utilization of picrosirus red staining and polarized light imaging. No significant differences were found between each of the bioinks. Although the 4:1 bioink was shown to be most ideal for cell elongation as demonstrated in the LIVE/DEAD, H&E, and picrosirus red staining images, it was previously shown to be problematic for printing itself. Therefore, the 3:1 bioink was used for printed liver microenvironments as it provided a greater amount of collagen to create physiological relevance and remained printable for a workable period of time.

To show a potential application of this bioink system, liver constructs containing primary human hepatocytes and liver stellate cells were bioprinted and employed in a straightforward drug toxicity test. Acetaminophen (APAP) is a widely used pain reliever that is well documented to cause liver damage upon overdosing and has been used as a test compound in other tissue engineered liver organoid studies [37]. Liver constructs were bioprinted using the 3:1 COL I to HA bioink. Additional printed structures were treated with APAP to show loss of function in comparison to healthy, untreated structures. Functionality was maintained for two weeks indicating the extrusion 3D bioprinting process with the bioink did not adversely affect cells. The liver model we developed acts as a simple microenvironment to support hepatocytes allowing for functionality levels previously seen in literature, likely due to the more physiologic environment [39].

The development of a simple bioink that is printable and contains physiologic components advances the state of bioprinting in that it allows researchers to modulate 3D matrices for their desired application. For a balance in both printability and collagen content, the 3:1 COL I to HA bioink was selected. To demonstrate properties of the bioink, a liver model was used, however, other organ systems can be modeled with such a biomaterial as collagen concentration can be tuned to the tissue of interest. The use of methacrylated and thiolated base materials allows for addition of functionalized proteins or molecules to further customize the bioink for specific applications. Simple modifications such as the addition of laminin or fibronectin can jump-start cellular adhesion or drive biochemical pathway activation. Certain disease phenotypes such as cancer or fibrosis are typified by changes in elastin and fibronectin levels which can be simulated through additions to the bioink backbone [40]. Because crosslinking is controlled through UV radiation, zones of different bioink formulations can be deposited in serial layers to simulate the varied layers of a physiologic tissue. For instance, a layer of elastin-functionalized COL I and -III bioink could be deposited and crosslinked to represent a dermal layer of skin upon which a laminin-enriched layer of collagen-IV bioink could be printed as the basement membrane of the epidermis [41]. Similar layered structures could be produced to represent colonic submucosa and epithelium or the layers of blood vessels. However, the bioink is still limited by its loss of homogeneity over time and its temperature sensitivity, and thus is restricted in the complexity of geometries and structures that can be printed. In addition, the uncrosslinked bioink has a low viscosity and relies on rapid UV-driven crosslinking to hold a printed shape. Low viscosity is also limiting in which shapes and structures can be printed as multilayer structures have not yet been achieved. Given these properties, the bioink will be

difficult to use for high resolution or high aspect printing. The problems associated with low viscosity can be mitigated by adding thickening agents to the formulation, but other hydrogel parameters may change as a result. These features—high resolution and high aspect ratio printing—are currently areas of focus in continuing research.

Conclusion

Conclusively, by combining methacrylated COL I with thiolated HA and UV crosslinker, a simple bioink that is both printable and physiologically relevant has been developed. It was hypothesized that combining two chemically modified materials commonly used for 3D matrices would create a hybrid bioink that allows for a material fluid enough to be printed and elastic enough to maintain its shape while also being advantageous for cell viability and interaction. Three bioink formulations were created and tested to determine ideal parameters for a simple 3D bioprinted liver model. Each of the formulations appeared to facilitate cell viability matching currently used biomatrices and some were shown to allow cell elongation. A 3:1 COL I to HA ratio was determined to be most ideal for printing and was utilized for the printing of the liver microenvironments. Using the bioink, structures containing primary human hepatocytes were printed and monitored over the course of 2 weeks during which time they were able to maintain urea and albumin production and responded appropriately to APAP. Such a bioink allows for modulation of collagen and hyaluronic acid as well as creating the opportunity for additional proteins and ECM components to be added. This collagen and HA hybrid bioink formulation could serve as a useful platform on which to build additional functionality, to provide a bioink system that has the potential to biofabricate a variety of tissue types for applications ranging from *in vitro* drug screens, disease modeling, and perhaps in the future, biomanufacturing of tissue products for human use.

Supplementary Material

Refer to Web version on PubMed Central for supplementary material.

Acknowledgments

The authors acknowledge funding from the Medical Technology Enterprise Consortium under Contract # W81XWH-15-9-0001. The views and conclusions contained herein are those of the authors and should not be interpreted as necessarily representing the official policies or endorsements, either expressed or implied of the US Government.

References

[1]. Mills M and Estes MK 2016 Physiologically relevant human tissue models for infectious diseases Drug Discovery Today 21 1540–52 [PubMed: 27352632]

[2]. Lancaster MA and Knoblich JA 2014 Organogenesis in a dish: modeling development and disease using organoid technologies Science 345 1247125 [PubMed: 25035496]

[3]. Skardal A, Shupe T and Atala A 2016 Organoid-on-a-chip and body-on-a-chip systems for drug screening and disease modeling Drug Discovery Today 21 1399–411 [PubMed: 27422270]

[4]. Pampaloni F, Reynaud EG and Stelzer EH 2007 The third dimension bridges the gap between cell culture and live tissue Nat. Rev. Mol. Cell Biol 8 839–45 [PubMed: 17684528]

[5]. Chia HN and Wu BM 2015 Recent advances in 3D printing of biomaterials J. Biol. Eng 9 4 [PubMed: 25866560]

[6]. Liu W. et al. 2017; Rapid continuous multimaterial extrusion bioprinting. Adv. Mater. 29:1604630.

[7]. Murphy SV and Atala A 2014 3D bioprinting of tissues and organs Nat. Biotechnol 32 773–85 [PubMed: 25093879]

[8]. Murphy SV, Skardal A and Atala A 2013 Evaluation of hydrogels for bio-printing applications J. Biomed. Mater. Res. A 101 272–84 [PubMed: 22941807]

[9]. Hospodiuk M, Dey M, Sosnoski D and Ozbolat IT 2017 The bioink: a comprehensive review on bioprintable materials Biotechnol. Adv 35 217–39 [PubMed: 28057483]

[10]. Ahmed EM 2015 Hydrogel: preparation, characterization, and applications: a review J. Adv. Res 6 105–21 [PubMed: 25750745]

[11]. Highley CB, Prestwich G D and Burdick J A 2016 Recent advances in hyaluronic acid hydrogels for biomedical applications Curr. Opin. Biotechnol 40 35–40 [PubMed: 26930175]

[12]. Skardal A and Atala A 2015 Biomaterials for integration with 3-d bioprinting Ann. Biomed. Eng 43 730–46 [PubMed: 25476164]

[13]. Delgado LM, Bayon Y, Pandit A and Zeugolis DI 2015 To cross-link or not to cross-link? Cross-linking associated foreign body response of collagen-based devices Tissue Eng. B 21 298–313

[14]. Ouyang L, Highley CB, Sun W and Burdick JA 2017 A generalizable strategy for the 3D bioprinting of hydrogels from nonviscous photo-crosslinkable inks Adv. Mater 29 1604983

[15]. Ehrbar M, Sala A, Lienemann P, Ranga A, Mosiewicz K, Bittermann A, Rizzi SC, Weber FE and Lutolf MP 2011 Elucidating the role of matrix stiffness in 3D cell migration and remodeling Biophys. J 100 284–93 [PubMed: 21244824]

[16]. Devarasetty M, Wang E, Soker S and Skardal A 2017 Mesenchymal stem cells support growth and organization of host-liver colorectal-tumor organoids and possibly resistance to chemotherapy Biofabrication 9 021002 [PubMed: 28589925]

[17]. Skardal A, Devarasetty M, Rodman C, Atala A and Soker S 2015 Liver-tumor hybrid organoids for modeling tumor growth and drug response *in vitro* Ann. Biomed. Eng 43 2361–73 [PubMed: 25777294]

[18]. Esch MB, Prot JM, Wang YI, Miller P, Llamas-Vidales JR, Naughton BA, Applegate DR and Shuler ML 2015 Multi-cellular 3D human primary liver cell culture elevates metabolic activity under fluidic flow Lab Chip 15 2269–77 [PubMed: 25857666]

[19]. Wrzesinski K, Rogowska-Wrzesinska A, Kanlaya R, Borkowski K, Schwammle V, Dai J, Joensen KE, Wojdyla K, Carvalho VB and Fey SJ 2014 The cultural divide: exponential growth in classical 2D and metabolic equilibrium in 3D environments PloS One 9 e106973 [PubMed: 25222612]

[20]. Lee J, Cuddihy MJ, Cater GM and Kotov NA 2009 Engineering liver tissue spheroids with inverted colloidal crystal scaffolds Biomaterials 30 4687–94 [PubMed: 19524294]

[21]. Godoy P et al. 2013 Recent advances in 2D and 3D *in vitro* systems using primary hepatocytes, alternative hepatocyte sources and non-parenchymal liver cells and their use in investigating mechanisms of hepatotoxicity, cell signaling and ADME Arch. Toxicol 87 1315–530 [PubMed: 23974980]

[22]. Yip D and Cho CH 2013 A multicellular 3D heterospheroid model of liver tumor and stromal cells in collagen gel for anti-cancer drug testing Biochem. Biophys. Res. Commun 433 327–32 [PubMed: 23501105]

[23]. Powers MJ et al. 2002 A microfabricated array bioreactor for perfused 3D liver culture Biotechnol. Bioeng 78 257–69 [PubMed: 11920442]

[24]. Yoon No D, Lee KH, Lee J and Lee SH 2015 3D liver models on a microplatform: well-defined culture, engineering of liver tissue and liver-on-a-chip Lab Chip 15 3822–37 [PubMed: 26279012]

[25]. Ruddell RG, Oakley F, Hussain Z, Yeung I, Bryan-Lluka LJ, Ramm GA and Mann DA 2006 A role for serotonin (5-HT) in hepatic stellate cell function and liver fibrosis Am. J. Pathol 169 861–76 [PubMed: 16936262]

[26]. Coulouarn C, Corlu A, Glaise D, Guenon I, Thorgeirsson SS and Clement B 2012 Hepatocyte-stellate cell cross-talk in the liver engenders a permissive inflammatory microenvironment that drives progression in hepatocellular carcinoma Cancer Res. 72 2533–42 [PubMed: 22419664]

[27]. Xu L, Hui A Y, Albanis E, Arthur M J, O'Byrne S M, Blaner W S, Mukherjee P, Friedman S L and Eng F J 2005 Human hepatic stellate cell lines, LX-1 and LX-2: new tools for analysis of hepatic fibrosis Gut 54 142–51 [PubMed: 15591520]

[28]. Schindelin J. et al. 2012; Fiji: an open-source platform for biological-image analysis. Nat. Methods. 9:676. [PubMed: 22743772]

[29]. Bartnikowski M, Wellard R M, Woodruff M and Klein T 2015 Tailoring hydrogel viscoelasticity with physical and chemical crosslinking Polymers 7 19

[30]. Munoz-Pinto DJ, Jimenez-Vergara AC, Gharat TP and Hahn MS 2015 Characterization of sequential collagen-poly (ethylene glycol) diacrylate interpenetrating networks and initial assessment of their potential for vascular tissue engineering Biomaterials 40 32–42 [PubMed: 25433604]

[31]. Hung KC, Tseng CS, Dai LG and Hsu SH 2016 Water-based polyurethane 3D printed scaffolds with controlled release function for customized cartilage tissue engineering Biomaterials 83 156–68 [PubMed: 26774563]

[32]. Skardal A, Zhang J, McCoard L, Xu X, Oottamasathien S and Prestwich GD 2010 Photocrosslinkable hyaluronan-gelatin hydrogels for two-step bioprinting Tissue Eng. A 16 2675–85

[33]. Camci-Unal G, Cuttica D, Annabi N, Demarchi D and Khademhosseini A 2013 Synthesis and characterization of hybrid hyaluronic acid-gelatin hydrogels Biomacromolecules 14 1085–92 [PubMed: 23419055]

[34]. Mederacke I, Hsu CC, Troeger JS, Huebener P, Mu X, Dapito DH, Pradere JP and Schwabe RF 2013 Fate tracing reveals hepatic stellate cells as dominant contributors to liver fibrosis independent of its aetiology Nat. Commun 4 2823 [PubMed: 24264436]

[35]. Mederacke I, Dapito DH, Affo S, Uchinami H and Schwabe RF 2015 High-yield and high-purity isolation of hepatic stellate cells from normal and fibrotic mouse livers Nat. Protocols 10 305–15 [PubMed: 25612230]

[36]. Bell CC. et al. 2016; Characterization of primary human hepatocyte spheroids as a model system for drug-induced liver injury, liver function and disease. Sci. Rep. 6:25187. [PubMed: 27143246]

[37]. Skardal A. et al. 2017; Multi-tissue interactions in an integrated three-tissue organ-on-a-chip platform. Sci. Rep. 7:8837. [PubMed: 28821762]

[38]. Lin N, Chen Z, Lu Y, Li Y, Hu K and Xu R 2015 Role of activated hepatic stellate cells in proliferation and metastasis of hepatocellular carcinoma Hepatol. Res 45 326–36 [PubMed: 24827154]

[39]. Skardal A, Devarasetty M, Soker S and Hall AR 2015 In situ patterned micro 3D liver constructs for parallel toxicology testing in a fluidic device Biofabrication 7 031001 [PubMed: 26355538]

[40]. Frantz C, Stewart KM and Weaver VM 2010 The extracellular matrix at a glance J. Cell Sci 123 4195–200 [PubMed: 21123617]

[41]. Briquez P, Hubbell JA and Martino M 2015 Extracellular matrix-inspired growth factor delivery systems for skin wound healing Adv. Wound Care 4 479–89

[42]. Bhise NS. et al. 2016; A liver-on-a-chip platform with bioprinted hepatic spheroids. Biofabrication. 8:014101. [PubMed: 26756674]

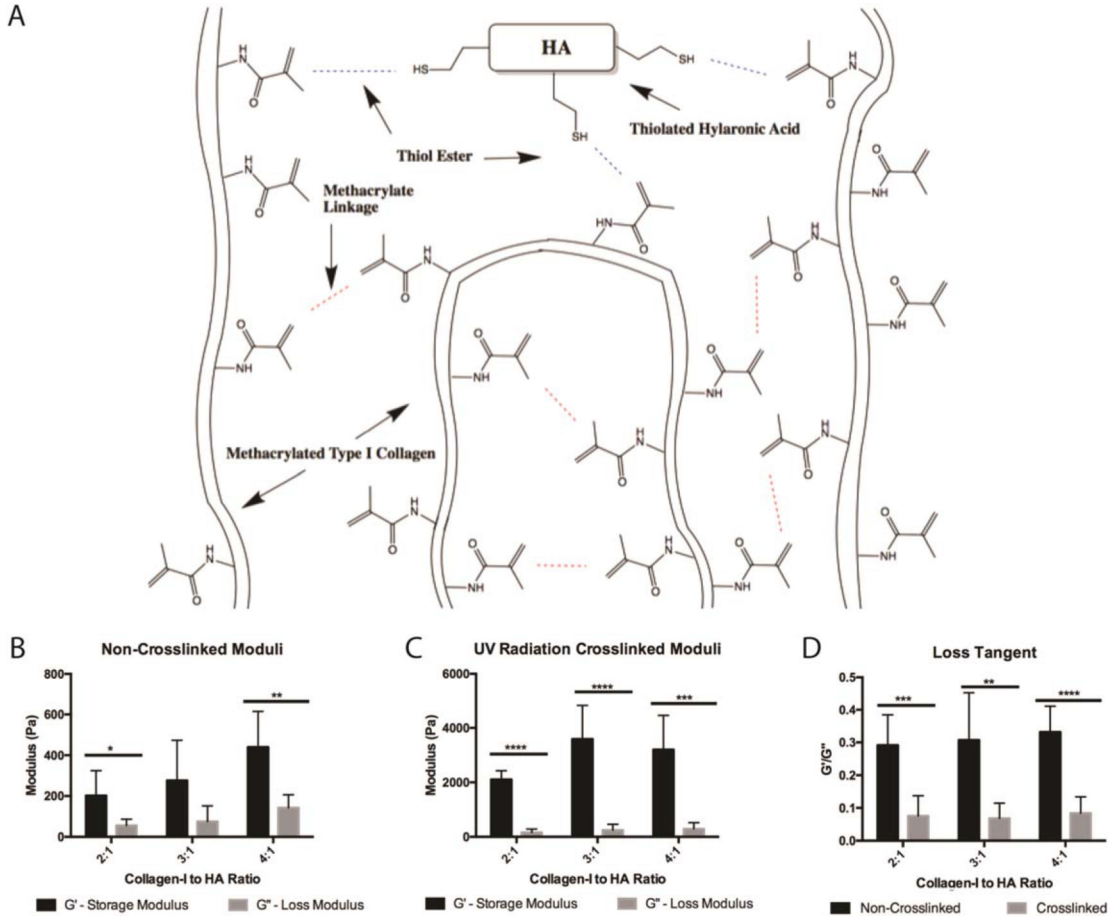

Figure 1.

Hybrid bioink characterization. (A) An illustration of hybrid bioink chemistry between thiolated hyaluronic acid and methacrylated collagen. UV radiation drives a thiol-ene reaction facilitated by the included photoinitiator. Additionally, methacrylate linkage occurs between COL I fibers to allow collagen–collagen binding. To characterize each bioink, **G′** and **G″**were measured for each formulation before crosslinking (B) and after printing and UV radiation crosslinking **(C).** Loss tangents (**G′**/**G″**) can be used as a measure of printability and were calculated for each formulation before and after crosslinking (D). Student's T-tests were performed to compare shear storage moduli between the non-crosslinked and crosslinked conditions for each biomaterial condition, non-crosslinked conditions were significantly different than the crosslinked conditions ($p < 0.005$) (B), (C). *: $p < 0.05$, **: $p < 0.01$, ***: $p < 0.005$, ****: $p < 0.001$.

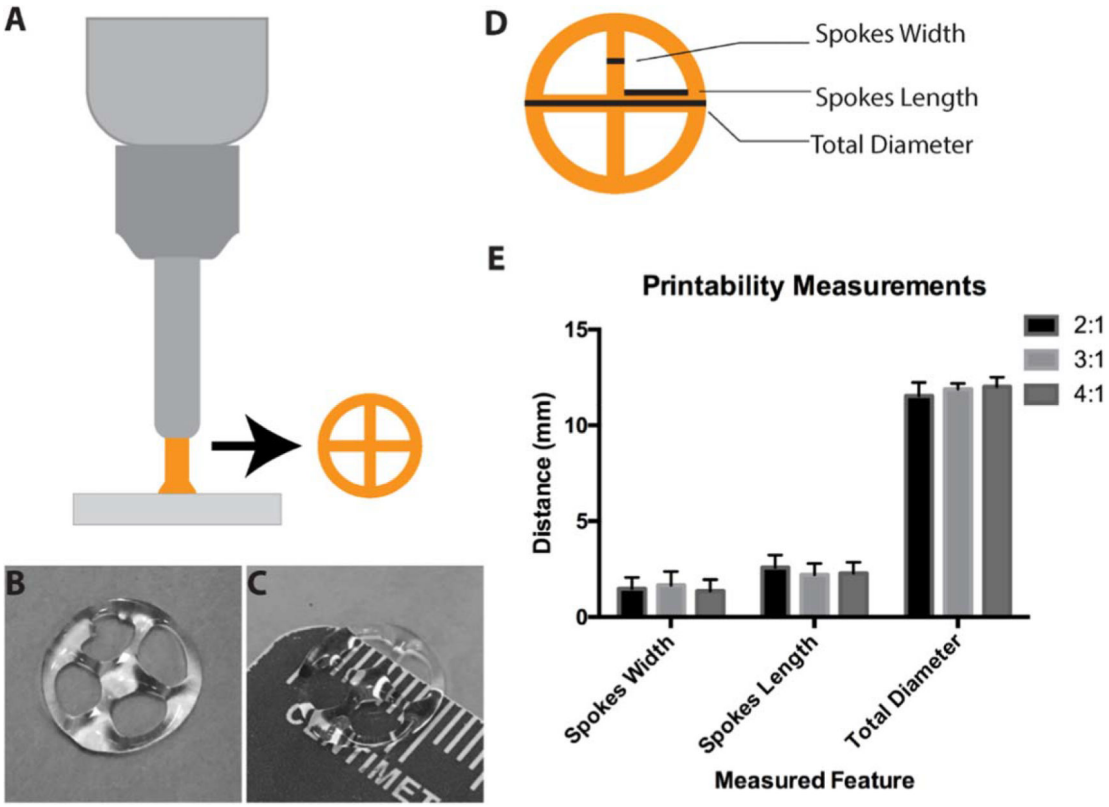

Figure 2.

Bioprinting of hybrid bioink and printability characterization. A desktop extrusion bioprinter was used to print a 4-spoke wheel structure (illustrated in (A), printed structure in (B), (C)). To assess the consistency of bioink printability, spoke width, spoke length, and wheel diameter (D) of printed structures were measured (E). All formulations displayed similar printability and consistency as there were no differences found in structure measurements between bioinks.

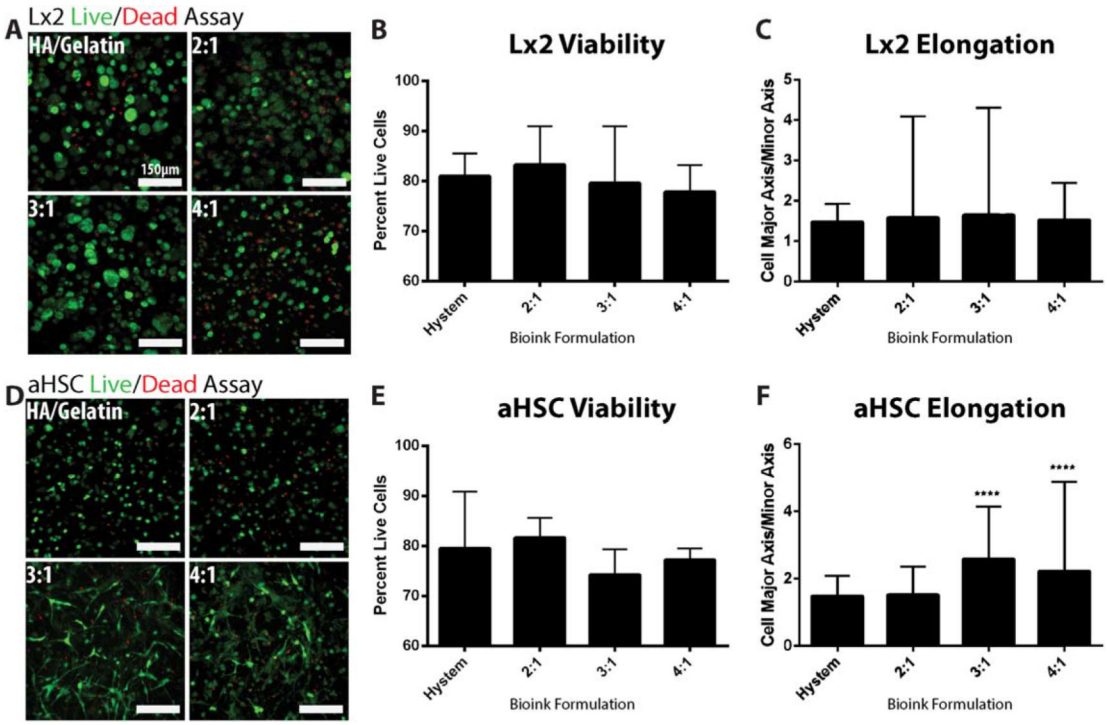

Figure 3.

Bioink biocompatibility and viability analysis. To assess the biocompatibility of bioink formulations, a Live/Dead assay was performed using L × 2 and aHSC cells. Representative images were taken of stained L × 2 cells (A) as well as stained aHSCs (D) in all three bioink formulations as well as a commercially available hyaluronic acid-gelatin hydrogel. Images were then manually quantified to determine percentage of lives cells for comparison of overall viability of L × 2 cells (B) and aHSCs (E). No differences were found in cell viability between bioink formulations. Morphological differences were quantified by measuring cellular aspect ratio (major axis/minor axis) for each condition (C), (F). ****: $p <$ 0.001 versus Hystem.

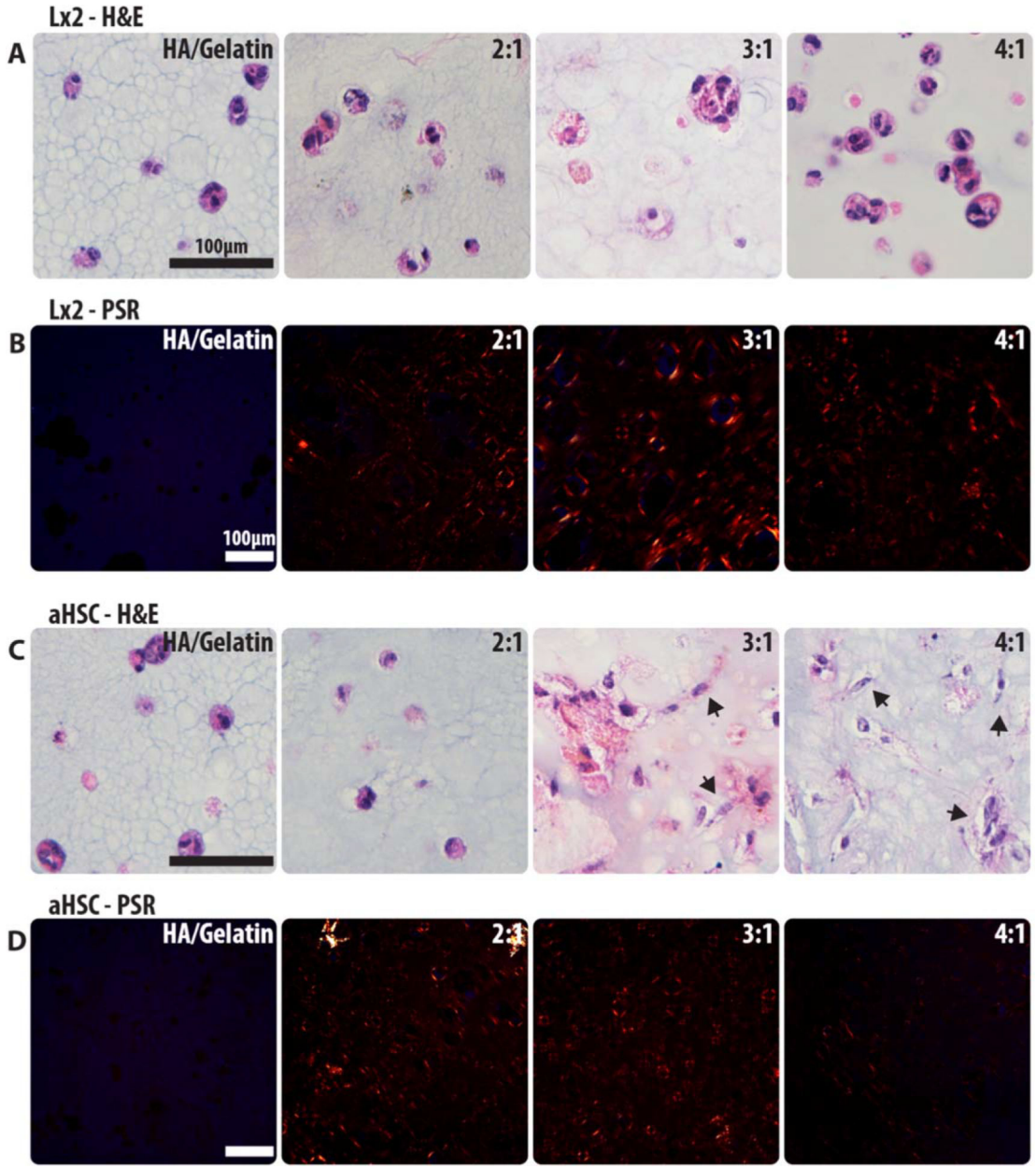

Figure 4.

Histological staining of cell–matrix interaction. H&E staining was performed on both the L × 2 and aHSC constructs to visualize cells within each bioink formulation (A), (C). Cells that exhibit matrix interaction will elongate (denoted by arrows). Picrosirus red staining was also performed to visualize collagen deposition and bundling (orange/red signal labels collagen) within the bioinks (B), (D). Deposited collagen will appear as short, random fibers, and red signal denotes bundled collagen.

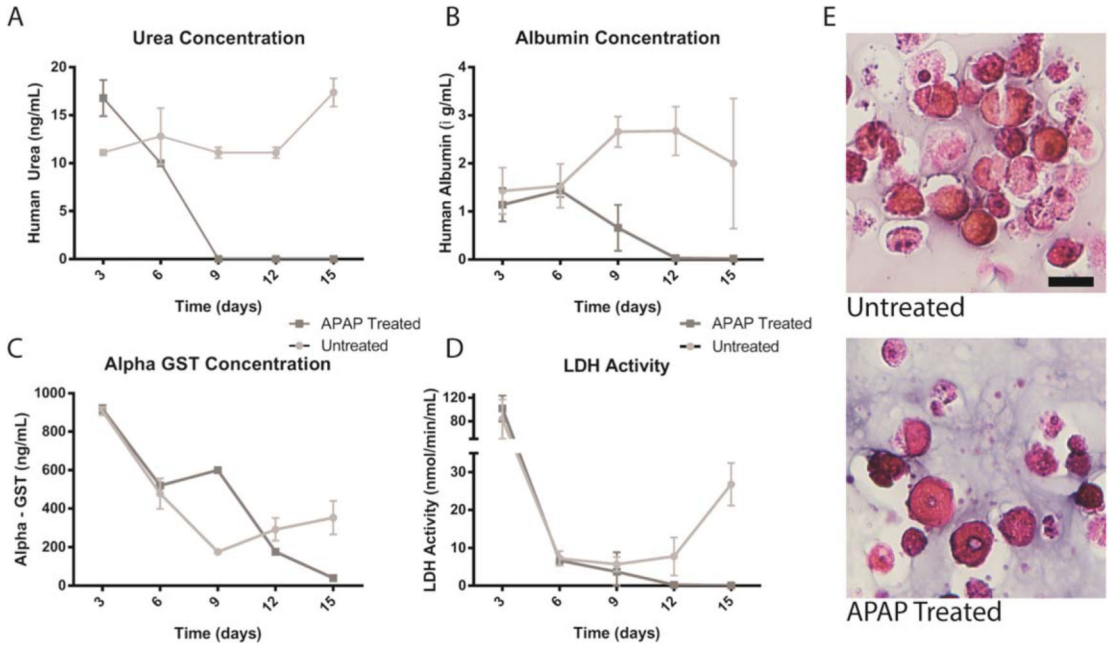

Figure 5.

Hepatocyte functionality with and without APAP Treatment. To assess the overall functionality of liver organoids, urea, albumin, α-GST, lactic acid dehydrogenase (LDH) were measured over time with and without APAP treatment, arrows denote time of treatment (A)–(D). H&E images of untreated and treated hepatocytes at the end of the study show change in cellularity and health of cells (E) indicating hepatocytes respond appropriately to APAP treatment. Scale bar—20 μm.